Flexible Nitrogen Doped SiC Nanoarray for Ultrafast Capacitive Energy Storage

Youqiang Chen,[*,†,‡] Xinni Zhang,[†,§] and Zhipeng Xie[§]

[†]College of Physics Science, Qingdao University, Qingdao, 266071, P. R. China, [‡]Department of Chemistry, Tsinghua University, Beijing 100084, P. R. China, and [§]State Key Lab of New Ceramics and Fine Processing, Tsinghua University, Beijing 100084, P. R. China

ABSTRACT The current trend with integrated energy-storage units in portable electronics lies in continuous advancements in nanostructured materials, thin-film manufacture technologies, and device architectures with enhanced functionality and reliability of existing components. Despite this, it is still challenging to provide cost-efficient solution to further improve the energy and power densities and cyclability of supercapacitors (SCs), especially at ultrafast rates while maintaining their environmentally friendly and even well-run at arbitrary harsh environments character. In this contribution, we report the fabrication of quasi-aligned single crystalline 3*C*-SiC nanowire (3*C*-SiCNW) array with tailored shapes and nitrogen-doping (N-doping). The resultant large-scale SiCNWs were directly grown on the surface of a flexible carbon fabric *via* a simple chemical vapor deposition method. We found that the SC performance of SiCNW arrays can be substantially enhanced by nitrogen doping, which could favor a more localized impurity state near the conduction band edge that greatly improves the quantum capacitance and hence increases the bulk capacitance and the high-power capability. The measured areal capacitances are higher with values of 4.8 and 4.7 mF cm^{-2}, in aqueous and gel electrolytes, respectively. The all-solid-state flexible textile-based SCs (TSCs) made with these electrodes are mechanically robust under bent and twisted states. Further, they show a power density of 72.3 mW cm^{-2} that is higher than that of electrolytic capacitors, and an energy density of 1.2×10^{-4} mW·h cm^{-2}, in association with superior rate ability, cyclability, and being environmentally friendly. Such SiCNW—TSC devices allow for operations at ultrahigh rate up to 30 V s^{-1}, 2 orders of magnitude higher than that of conventional supercapacitors. All these data are comparable to the reported results for 1D nanostructure-based carbon nanotubes (CNTs) or graphenes, thus showing the promising application as large-area flexible textile electronics.

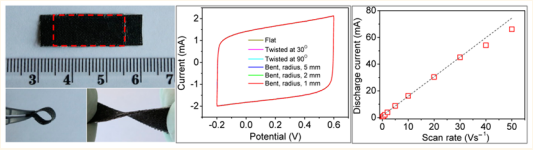

KEYWORDS: SiC · nanowires · supercapacitors · flexible · energy storage

With new forms of next generation portable flexible electronics like curved smartphones, e-paper, conformal skin sensors, and even various wearable electronics emerging, there is a pressing need for the development of flexible energy conversion and storage sources like electrochemical capacitors by which the energy is stored by charging electrical double layers through highly reversible ion electrosorption on the surface of high-surface-area electrodes.[1,2] Supercapacitors (SCs) have great potential to complement or replace batteries and electrolytic capacitors since they typically deliver a power density that is of an order magnitude larger (10 kW kg^{-1}) than that of lithium ion batteries renowned for their great successes in modern materials electrochemistry, and an energy density that is of two orders magnitude higher (10 W·h kg^{-1}) than that of electrolytic capacitors.[1,3] Although much progress has been achieved with an in-depth understanding of charge storage mechanisms by tailoring various functional materials,[4−14] it is still tricky to further improve the energy and power densities and cyclability of SCs, especially at ultrafast rates of around 3.6 ms while maintaining their environmentally friendly and even well-run at arbitrary harsh environments character; you have to search for a robust material that is nearly full-featured as much as possible.

Due to the potential of nanotechnology, which promises to change electronics' industry, ushering in flexible devices, and even computers that can interface with the cells in your body, researchers have zeroed in on how to increase the energy and power densities of flexible macro-/micro-supercapacitors *via* the fabrication of excellent low-dimensional nanostructured electroactive materials, the most promising kind of which includes carbonaceous materials (carbon nanotube (CNT)[15,16] and graphene[17,18]), semiconductor nanostructures,[19,20] transition metal oxides (ruthenium oxide[21] and manganese oxide[22]) and conductive polymers (polypyrrole[23] and polyaniline[24]), *etc*. However, fabrication of

* Address correspondence to chen-yq06@mails.tsinghua.edu.cn.

Received for review March 24, 2015 and accepted August 3, 2015.

Published online August 10, 2015
10.1021/acsnano.5b01784

such highly efficient SCs with ultrafast rates has been extremely inefficient from both technology and theory points of view, not to mention that none of them can withstand harsh conditions and/or being environmentally friendly, *etc*. In just the most newly impressive instance, the methane-plasma treatment graphene film was used in flexible thin-film in-plane microsupercapacitors with several square centimeter footprints; the films gave respectable areal and volumetric capacitance, as well as high power density (495 W cm^{-3}), but it involved a tedious methane-plasma treatment and transfer process coupled with lithography techniques that were applied to manufacture graphene-based interdigital microelectrode patterns.[18] In addition, it follows only double-layer capacitance operative mechanism with inevitable molecular diffusion and sieving effects. The impaired ion transport in subnanometer pores becomes even more pronounced when graphene-based compact electrodes are made thicker, limiting the achievable value of a power density, owing to their intrinsic microcorrugated two-dimensional configuration and self-assembly behavior. Nanoarchitectured hybrids have been made so far to increase both energy and power performances, but many are not yet compatible with standard flexible microfabrication protocols. Also they suffer from many limitations, such as restricted cycle life, fast decayed capacitance at high rates, abrupt failure and poor low-temperature kinetics that are associated with relatively sluggish electrochemical charge-transfer kinetics, which are by no means of the thermodynamic steady states in SCs.[25]

Generally, the presence of abundant microchannels in a random network degrades power density, whereas the absence of mesopores puts a limit on charging–discharging rates.[26] To overcome this most vexing problem, well-aligned nanoarrays have been used for high-performance SCs, which revealed extremely small relaxation time constants that drives a linear current increase up to ultrahigh scan rates.[26] In theory, the drawback of the low-frequency response SC is a direct result of using porous electrodes that can arise by storing charge in a distributed fashion with associated ionic resistance.[18] This leads to the energy and power density trade off each other to fit themselves to micro- and mesoporous structures, which also relies on the mass density in a SC electrode. For instance, at the low coverage of porous structures, ultrafast devices can be achieved with an extremely low relaxation time constant (*e.g.*, 0.2 and 0.238 ms using oriented graphene[26] and reduced graphene oxide), but the low capacitances and energy densities per unit area/volume are expected; *vice versa* the higher energy densities at a high coverage. While careful optimization must be made to overcome this trade-off characteristic for the advantageous aligned nanoarrays, there are chances to partially get around the effect with the quantum capacitance. The most recent study hints the quantum capacitance could be a limiting factor for the interfacial capacitance of porous network, which strongly correlates with Fermi electronic states rather than double-layer capacitances that are solely calculated on the basis of a material's surface area.[27]

Another critical issue for the high-performance flexible SCs is matching the SC substrate for the nanoarray growth while attaining a mechanical robust system. As of now, most flexible SCs have been involving three types of substrates such as carbon fabric,[28] graphene/CNT,[15,18] and polymer films.[17,18] Though the easy-use clear plastic sheet (*e.g.*, polyethylene terephthalate) is lightweight and affordable to virtually many micro-in-plane electronics, it is generally not electrical/thermal conductive, not to mention its extremely unstable property toward a high-temperature application. While films made of graphene/CNT or their mixtures are excellent at conducting heat and charge, they are nevertheless too thin to hold their own against intense mechanical deformation, and as such can be used merely as a transitional substrate. By contrast, a highly flexible, reticulate, woven carbon-based structure is an amazing kind of substrate that can circumvent this slew of drawbacks with an ion permeating macroporous highway scaffold since working in its favor is it is highly conductive and can endure very high temperatures, and therefore, the wisest choice is to seamlessly integrate a competitive NW-based architecture onto its flexible surface with precisely control over the NW growth conditions.[28]

In consideration of the problems described above, researchers have thus far continuously dedicated their efforts to searching for a single cost-effective energy-storage-system of the most integrated merits to fabricate the flexible nanostructure-based textile-supercapacitors (TSCs).

The silicon carbide (SiC) 1D nanostructure, compelling in an ability to be bent, charged and dunked, is one of the most promising semiconductors in many areas of futuristic nanoscience and technology.[29] In fact, SiC 1D nanostructures have demonstrated potential to meet nearly any stringent requirement to be an ideal functional elements in nanoelectronics.[30−32] Central to their excellent properties that outperform many other semiconductor NWs is their outstanding mechanical properties, breakdown field strength, and radiation resistance, as well as exclusive high thermal conductivity and electron affinity, making them useful for widespread applications in electronics and short-wavelength optics, in particular, in high-temperature/high-voltage/chemically harsh environments. Moreover, this environmentally friendly and superior-in-arbitrary-environment SiC possesses an indirect large bandgap (E_g: 2.36−3.23 eV) along with a high electron mobility in the bulk, where the localized states can be best tuned by varying the effective work function *via* a doping strategy.[33−35] Most recently,

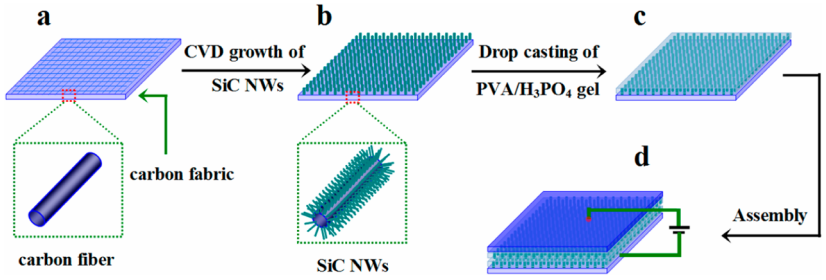

Figure 1. Schematic illustration showing the fabrication process for a SiCNW−TSC. (a and b) SiC nanowire growth with the catalysis-assisted high-temperature pyrolysis at 1550 °C, for 30 min under mixed ultrahigh purity N_2 (99.99%)/Ar (99.99%) on the carbon fabric. (c) Drop casting and solidification of the PVA/H_3PO_4 gelled electrolyte on the surface-modified substrate. (d) Assembly of sandwich geometry of the flexible SiCNW−TSCs.

Roya Maboudian and others reported for the micro-supercapacitor properties of 3*C*-SiC NW arrays, which demonstrate comparable values reported for planar micro-supercapacitor CNT based electrodes.[36] However, their work is only limited to a rigid in-plane SiC thin film; highly flexible SiC NW array based SCs have scarcely been reported to date.

Herein, we report the fabrication of quasi-aligned single crystalline 3*C*-SiC nanowire (3*C*-SiCNW) array with tailored shapes and nitrogen-doping (N-doping). The resultant large-scale SiCNWs were directly grown on the surface of a flexible carbon fabric *via* a simple chemical vapor deposition method. We found that the SC performance of SiCNW−TSCs can be substantially enhanced by nitrogen doping. The as-synthesized flexible nanostructure arrays exhibit an excellent SC capacity, rate ability, and cyclability, which are comparable to the reported data for 1D nanostructure-based CNTs or graphenes.

RESULTS AND DISCUSSION

Fabrication of SiC NW Array Flexible Supercapacitors. The catalysis-assisted high-temperature pyrolysis is a facile technology that makes nanowire array direct growth onto the surface of the carbon fabric (CF) using the CVD method as schematically illustrated in Figure 1. This is associated with significant changes in the optical properties. For example, CF changes from a dark gray color to a light green-blue, which is a direct impact of SiCNW array growth as shown in the optical microscope images, Figure S1. We and others originally found precision of an *n*-type doping process, in which a string of doped SiCNW (*d*-SiCNW) arrays can be attained by accurately tuned *via* controlling the fraction of the inserted nitrogen atmosphere.[29] Moreover, the carbon fabric still preserves its excellent mechanical flexibility after SiCNW growth at high temperature and can even be twisted and rolled up periodically without any noticeable structural destruction, which can thus ensure the full electrical connection across multicircuits on rollable SCs or curved electronic devices even after being bent out of shape numerous times. Figure 2a shows the quasi-aligned growth of nanoarrays after treating CF with the pyrolysis-based CVD *via* a well-controlled Co-assisted vapor−liquid−solid (VLS) growth process[29,33] that enables full ion access to the electrode surface, which is essential for charging the electrodes.[28,36] The diameters at central parts of the *d*-SiCNWs range from 100 to 300 nm with an average wire length of ∼12 μm. *d*-SiCNWs also show under high-magnification smooth nanostructure surfaces and clear tips with a hexagonal cross section perpendicular to the axial growth direction, Figure S2. Figure 2c presents a typical XRD pattern of the resultant products, where the three major characteristic strong (111), (220), and (311) lattice plane peaks suggest the only crystalline phase of 3*C*-SiC (JCPSD card no. 29-1129) and the well crystallized as-grown nanowires. Further electron microscope observations from the SAED pattern, Figure 2d (the marked area A in Figure S3), which shows sharp diffraction spots suggest that the wires have the 3*C*-SiC structure with a single-crystalline nature, whereas a representative HRTEM image of the as-synthesized nanostructure implies its crystalline structure with a few defects such as stacking faults and twins, Figure 2f. The continuous well-resolved lattice fringes throughout the wire give additional evidence that the wires are crystalline and are commensurate with the (111) plane of 3*C*-SiC with a lattice spacing of 0.25 nm. Both the HRTEM image and SAED pattern suggest that the nanowires grow along the [111] direction, which is evidently due to only {111} surfaces being the most energetically favorable during the NW growth.[29] Figure 2e (the marked area B in Figure S3) is a typical EDS spectrum of the wire, which reveals the abundant elemental signature of Si and C with 1:1 atomic ratio of Si to C along with minor N, again demonstrating the nanostructure is made of SiC. Further evidence for N-doping within the wire is shown in the X-ray photoelectron survey spectrum of *d*-SiCNWs, Figure 3. And while the O 1s spectrum with a peak at ∼532 eV mainly rises from absorbed water on the surfaces of SiC nanostructures, the two strong peaks centered at ∼102.6 eV with an symmetric shape and ∼284.7 eV are attributed to Si 2p and C 1s core levels, corresponding to Si and C boned in the SiC

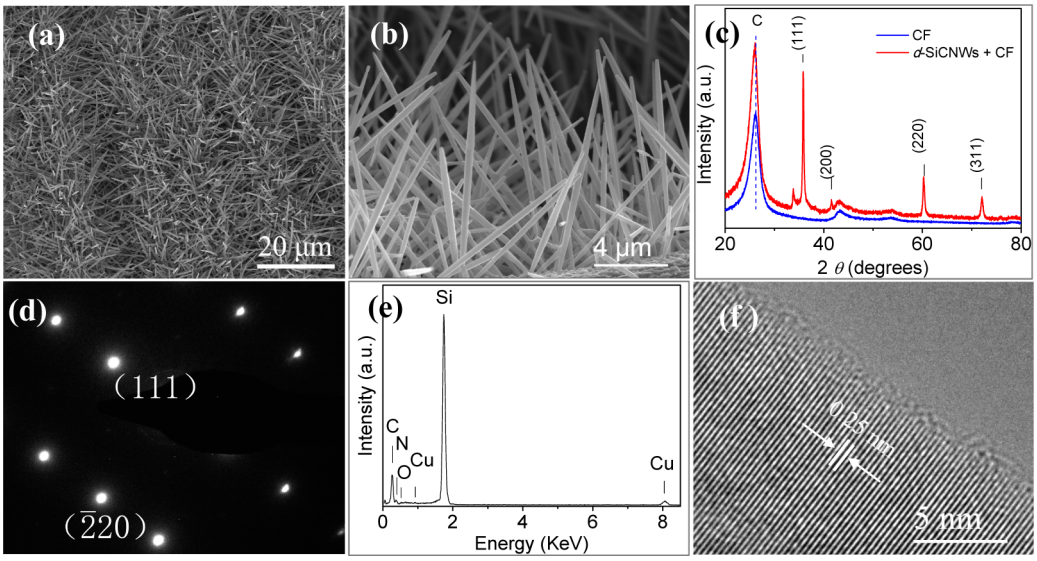

Figure 2. Characterization of *d*-SiCNWs. (a and b) Typical SEM images of the carbon fabric after reaction under different magnifications. (c) Representative XRD pattern recorded from the carbon fabric and as-synthesized *d*-SiCNWs on it. (d–f) Representative SAED pattern, corresponding EDS spectrum, and HRTEM image taken from a *d*-SiCNW.

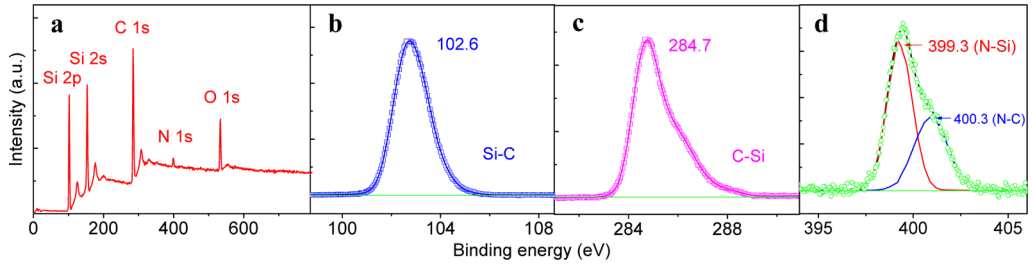

Figure 3. XPS characterization of *d*-SiCNWs. (a) XPS survey spectra along with the spectra of (b) Si 2p, (c) C 1s, and (d) N 1s.

lattice, which entirely reflect *n*-type doping characteristics of the wire.[37] Additionally, N 1s peaks centered at ~399.3 and 400.3 eV in Figure 3d are clearly observed, further revealing N-doping in the crystal lattices of SiC nanostructures. According to the XPS survey, the measured N dopant atomic concentration in the superficial layer of the wire is approximately ~3 atom % (note that all *d*-SiCNWs elsewhere typically correspond to ones with this data and the wire length of ~12 μm unless other stated), while those for the control (*c*-SiCNWs) and other doped nanostructure series with the same single-crystalline 3C-SiC structure were determined to be ~0, ~ 2, and ~5 atom %, respectively (Figures S4–S8, Table S1), which are consistent with their coprresponding bulk N dopant atomic concentration.

Conductivity Characterization of TSCs. Analysis of the cross section of the TSC reveals a thickness of 80 μm. For comparison, *I*–*V* tests were carried out for both an intrinsic and a nitrogen doped SiCNW as shown in Figure 4, panels a and b, respectively. The *c*-SiCNW exhibits linear and symmetric behavior, with a poor conductivity of 28.8 S m^{-1}, demonstrating its limit as an efficient current element. The *d*-SiCNW results in slightly nonlinear and symmetric behavior, with greatly improved conductivity, ranging from 7 $\times$ 10^3 to 8.6 $\times$ 10^3 S m^{-1}, superior to that of the state-of-the-art laser-reduced graphene films (1.7 $\times$ 10^3 S m^{-1}, thickness: ~ 10 μm), thus underscoring its great advantage in the excellent SC application. On the other hand, the pyrolysis-based NW growth process also retains its excellent electrical properties of the carbon fabric (Figure S9), which is essential for charging electrodes. Due to its high electrical conductivity and exceptionally high surface area, SiCNW arrays can serve as both the electrode material and current collector without the need for any additional binders or conductive additives getting in the way. This simplifies the fabrication process and results in lightweight cost-effective flexible TSCs.

Is Nitrogen Doping Crucial for the Performance of SiCNW–TSCs?. The superior performance of our prototype *d*-SiCNW–TSCs (~3 atom % N) for electrochemical energy storage was first tested at scan rates ranging from 10 to 20 000 mV s^{-1}, in an aqueous electrolyte of KCl, Figure 5a–c. The comparison between the cyclic voltammetry (CV) of the carbon fabric and *d*-SiCNW electrodes at a scan rate of 1000 mV s^{-1} reveals that CF only contributes very small capacitance to the electrodes. The cyclic voltammetry profiles are all rectangular in shape, suggesting the formation of an efficient

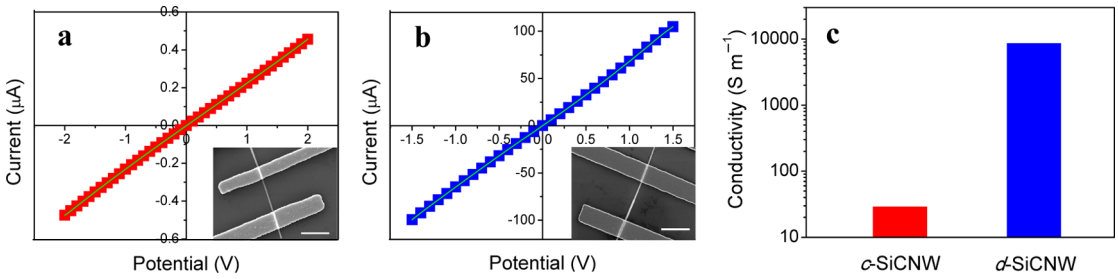

Figure 4. Conductivity characterization of SiCNWs. (a and b) *I*−*V* curves of a *c*-SiCNW and a *d*-SiCNW, respectively. The *d*-SiCNW exhibits a current enhanced by about 2 orders of magnitude, confirming the transition from nearly insulating *c*-SiCNWs to conducting doped *d*-SiCNWs. Inset: typical FET SEM images of their corresponding devices. Scale bar, 2 μm. (c) A comparison of their electrical conductivity values.

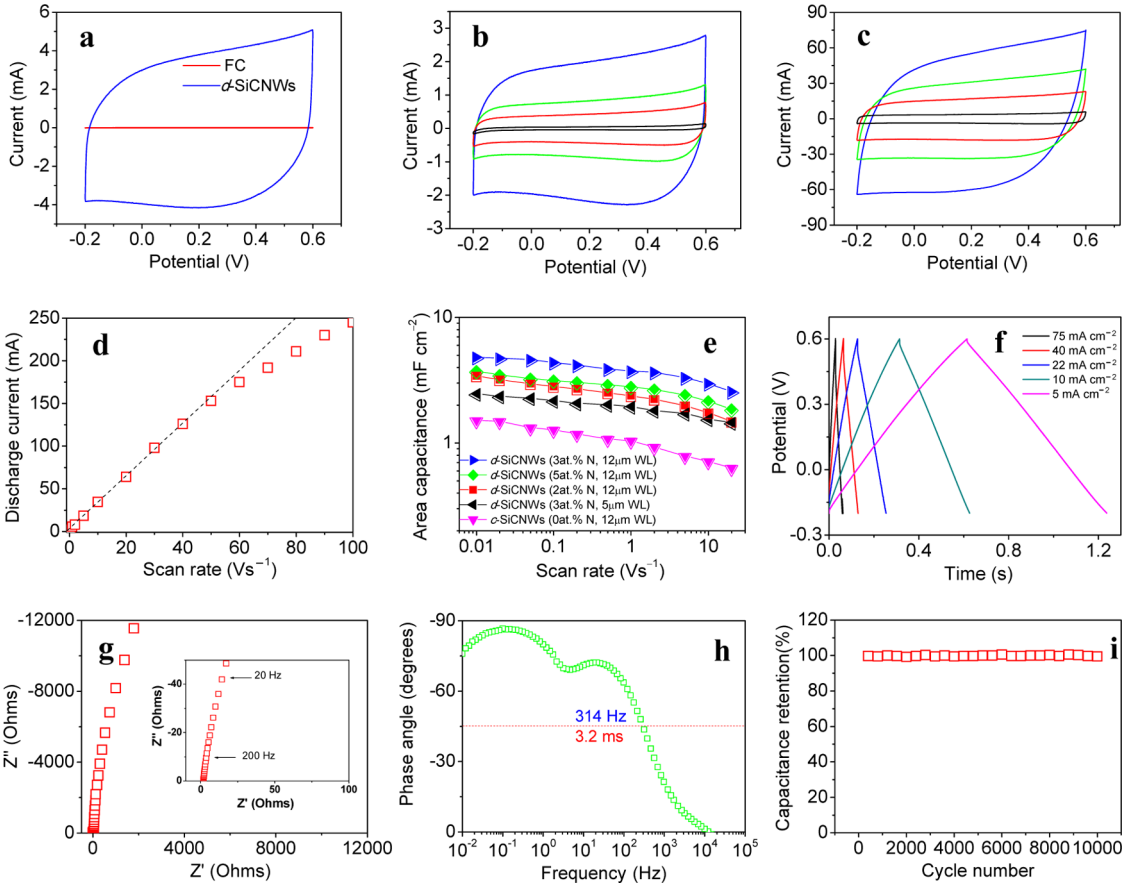

Figure 5. Electrochemical performance of *d*-SiCNW electrodes in aqueous electrolyte. (a−c) CV profiles of the carbon fabric and *d*-SiCNW electrodes at a scan rate of 1000 mV s^{-1}, and *d*-SiCNW electrodes at scan rates ranging from 10 to 20 000 mV s^{-1} ((b) 10 (black), 100 (red), 200 (green), 500 mV s^{-1} (blue); (c) 1000 (black), 5000 (red), 10 000 (green), 20 000 mV s^{-1} (blue)). (d) A plot of the discharge current as a function of the scan rate (red square line). Linear dependence (dashed line) is observed up to at least 50 000 mV s^{-1}, suggesting the ultrahigh power ability of *d*-SiCNW electrodes. (e) Evolution of the specific capacitance of SiCNW based SCs as a function of the scan rate, dopant , and wire length, respectively. (f) Galvanostatic charge/discharge curves of supercapacitors, operated with current densities ranging from 5 to 75 mA cm^{-2}. (g) Complex plane plot of the impedance with a magnification of the high-frequency region is provided in the inset. (h) Impedance phase angle *versus* frequency. (i) *d*-SiCNW electrodes show excellent stability at a scan rate of 1000 mV s^{-1}, losing only about 2% of its initial capacitance over 10 000 cycles.

EDL capacitor and fast charge propagation within the wire architecture. Even at an ultrafast scan rate of 20 000 mV s^{-1}, the CV remains nearly rectangular in shape, indicating the typical high-power capability of this nanoarray-based TSC. This coincides with a linear dependence of the discharge current on the scan rate kept over a wide range at least up to 50 000 mV s^{-1}, Figure 5d. Such rate performance promises 1 order of magnitude higher than that of electric double-layer capacitors.[18,38]

To shed light on the important role of doping, we compared the *d*-SiCNW electrodes with their undoped pristine counterpart, *c*-SiCNWs, with similar nanoarray morphologies, distribution patterns (Figures S5a−S8a),

and porous structures (Figure S10). Although SiCNWs's dopant concentrations or wire lengths (WL) are different with respect to each other, all well-defined large-scale nanoarrays clearly show a very similar nitrogen adsorption/desorption isotherms (type IV, according to IUPAC 1985 classification) and pore size distribution (PSD) that was calculated from the adsorption branch of the isotherm through standard nitrogen adsorption analysis using the Barret–Joyner–Halenda (BJH) method (Table S2). The PSD curve indicates the presence of macro- and mesopores with rare micropores and has a maximum at the pore diameter of ~45 nm. By maintaining essentially the same porous structure for all nanoarrays, any variance in their electrochemical performance can be traced to the dopant effect.

The areal capacitances of typical *d*-SiCNWs (~3 atom % N) were calculated to be 3.7 mF cm^{-2} at the scan rate of 1000 mV s^{-1}, with the highest specific capacitance of 4.8 mF cm^{-2} at the scan rate of 10 mV s^{-1}, respectively, both of which are larger than those of *d*-SiCNWs with lower and higher dopant concentrations (~2 and ~5 atom %), as well as a shorter wire length (~5 μm), Figures S11–S14. Specifically, these optimized values are much higher than those of *c*-SiCNWs: 0.95 and 1.22 mF cm^{-2}, suggesting the superior features of *d*-SiCNWs compared to *c*-SiCNWs, Figure S14. The present results for *d*-SiCNWs are also 1 magnitude higher than the values reported for SiC nanoarrays in the literature at lower scan rates: in-plane micro-supercapacitors (~0.24 mF cm^{-2}).[36] When the scan rate changed from 10 to 1000 mV s^{-1}, the *d*-SiCNW electrode retained ~77% of its capacitance, exhibiting a higher rate capacitance even operated at ultrahigh charge/discharge rates, Figure 5e. Even at an ultrafast rate of 20 000 m V s^{-1}, *d*-SiCNWs still delivered an areal capacitance of 2.38 mF cm^{-2}; in marked contrast, *c*-SiCNWs gave such capacitance of only 0.62 mF cm^{-2} under the same condition. The excellent performance of *d*-SiCNWs can be explained by the unique macro- and mesoscale-ordered pores of interstitial regions within the array packing structure of *d*-SiCNWs, which helps minimize the pathway for ion diffusion from the electrolyte to the electrode material on the relevant time scale. Another critical factor accounting for the discrepancy is associated with nitrogen-doping.[27] This effect results in an increase of electrical conductivity of *d*-SiCNWs with increasing dopant concentration, hence enhancing its rate ability and interfacial capacitance of the system. Moreover, the enhanced quantum capacitance induced by doping can greatly increase the bulk capacitance of TSCs without sacrificing its high-power capability since *n*-type nitrogen-doping provides an effective way to increase the density of the electronic states within SiCNWs, which entirely excludes diffusion and sieving effects.[29] The relatively lower capacitance of the most heavily doping (~5 atom %) compared to the optimized condition is not well understood, but it may be due to the imperfect crystalline structure in the SiCNWs (Figure S8), where the basal plane defects can act as low-energy electron traps, which can both shorten the carrier decay lifetime and reduce the SiCNW conductivity. It is instructive to note that although *d*-SiCNWs of ~5 μm WL at a lower coverage of porous structure exhibit higher ultrafast rate over the advantageous aligned nanoarrays of ~12 μm WL (~82% of capacitance retained at 1000 mV s^{-1}),[39] overall the latter displays better by partially overcoming the trade-off characteristic between capacitances and energy densities with excellent *n*-type conductivity and enhanced quantum capacitances. These results are further confirmed by galvanostatic profiles with current densities, ranging from 0.16 to 75 mA cm^{-2}, Figures 5f and S15. For instance, the curve regardless of an ultrahigh current density, 40 mA cm^{-2}, remains a nearly ideal triangular charge/discharge shape with only a smaller IR drop (0.018 V) and longer discharge time (~0.1 s), again confirming a low internal SC resistance and ultrafast capacitive capability of the *d*-SiCNW electrode.

Electrochemical impedance spectroscopy (EIS) further confirms the superior power performance of the *d*-SiCNW electrode, which was carried out at open circuit potential with an ac perturbation of 5 mV in the frequency range of 1000 kHz to 0.01 Hz. The complex-plane plot of impedance of the *d*-SiCNW electrode shows pure capacitive behavior even at high frequencies (200 Hz) owing to the highly accessible surface of the *d*-SiCNW, Figure 5g. The equivalent series resistance (ESR) obtained from the intercept of the plot on the real axis is only 1.7 Ω cm^{-2}, made manifest by the good ionic conductivity of the electrolyte and the low internal resistance of the nanoarray electrode. Remarkably, the *d*-SiCNWs show superior frequency response with an extremely small relaxation time (RC time constant), 3.2 ms, in comparison with 33 ms for the reported graphene based electrodes,[17] 3.2 ms for the SiNWs-based microsupercapacitor,[20] and 1.1 ms for the electrolytic capacitor, Figure 5h. The results clearly demonstrate the *d*-SiCNW array displays favorable ultrafast charge-transfer and fast electron transport kinetics, thus exhibiting a dramatically enhanced power performance of SCs. Furthermore, the *d*-SiCNWs shows excellent cycling stability, retaining 98% of its initial performance after 10 000 charge/discharge cycles, Figure 5i.

Bendable and Twistable *d*-SiCNW–TSCs. Currently at the forefront in electronics are roll-up displays, e-paper, smart sensors, transparent radio frequency identifications and even wearable electronics that represent new challenges in providing cost-efficient solutions to their large-area applications. The combination of a polymer matrix (*e.g.*, PVA) with the liquid electrolyte preserves the main attributes of an aqueous electrolyte (*e.g.*, H_3PO_4) by forming a PVA-H_3PO_4 gel electrolyte,

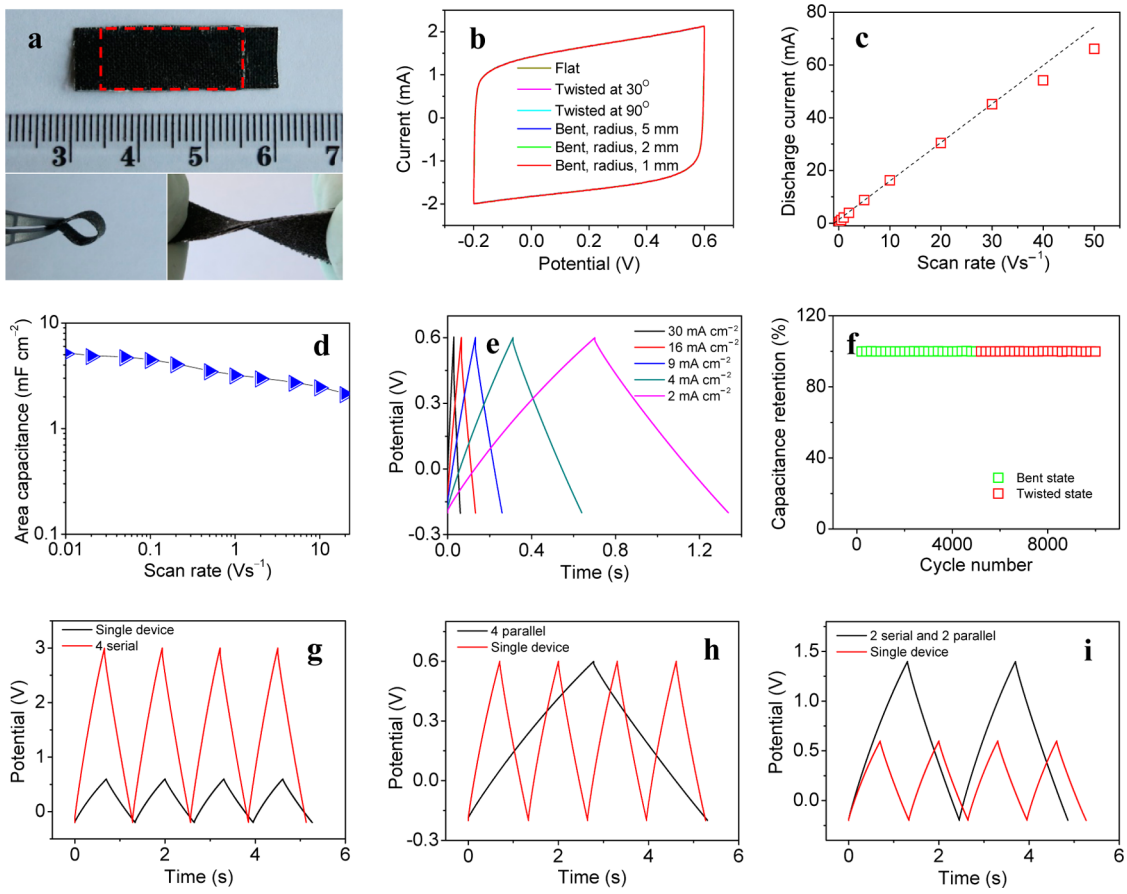

Figure 6. Electrochemical performance of a flexible, all-solid-state *d*-SiNW-TSC. (a) A digital photograph of the all-solid-state *d*-SiNW-device, with flat (top), bending (bottom left) and twisting states (bottom right). (b) CV profiles under different bending and twisting states at the scan rate of 1000 mV s^{-1}. (c) A plot of the discharge current as a function of the scan rate (red square). Linear dependence (dashed line) is observed up to at least 30 000 mV s^{-1}, suggesting the ultrahigh power ability of *d*-SiNW-TSCs. (d) Evolution of the specific capacitance of the supercapacitor as a function of the scan rate. (e) Galvanostatic charge/discharge curves of TSC, operated with current densities ranging from 2 to 30 mA cm^{-2}. (f) The *d*-SiNW-TSC shows excellent stability under bent (green) and twisted (red) states, at a scan rate of 1000 mV s^{-1}, losing only about 2% of its initial capacitance over 10 000 cycles. (g–i) Galvanostatic charge/discharge curves for four tandem TSCs connected in series (g), in parallel (h), and in a combination of series and parallel (i). A single device is shown for comparison.

while allowing easy shaping of the device without harmful leakage problems. On the other hand, the fabrication of nanoarrary-based supercapacitors on flexible substrates using current microfabrication, printing and electrochemical techniques does not appear to be suitable for highly flexible TSCs. In fact, the capacitive performance of SiC nanoarray has scarcely been examined under intense strain conditions such as bending or twisting. As demonstrated in Figures 6 and S16, the electrochemical performance for the all-solid-state *d*-SiCNW–TSC behaves in a similar way as those obtained with an aqueous electrolyte even at ultrahigh charge/discharge rates. For instance, a linear dependence of the discharge current on the scan rate remains up to nearly 30 V s^{-1}, Figure 6c. In addition, the TSC achieved an areal capacitance of 4.7 mF cm^{-2} at the scan rate of 10 mV s^{-1} and retained ~62% of this value at an ultrahigh rate, 1000 mV s^{-1}, Figure 6d. This is superior to the values reported for other flexible TSCs, but measured at much lower charge/discharge rates: H–TiO_2/MnO_2 NWs (54.6%, 200 mV s^{-1})[40] and WO_{3-x}/Au/MnO_2 NWs (~50%, 100 mV s^{-1}).[28] This is most relevant with the almost ideal triangular charge/discharge profiles and EIS data, which show smaller IR drops at ultrafast charge/discharge rates and a lower equivalent series resistance of only 2.7 Ω cm^{-2}, Figures 6e and S17. The RC time constant of the *d*-SiCNW–TSC was estimated to be 5.2 ms, much lower than that for the commercial AC-SC (10 000 ms) and carbon nanoparticles/MnO_2 nanorods flexible SC (500 ms),[22] and thus very promising compared with previously reported values for nanostructured planar micro-supercapacitors: activated carbon (700 ms),[38] onion-like carbon (26 ms),[38] and graphene/CNT composite (4.8 ms).[41]

In some aspects, the high-rate performance of our TSCs can be accounted for similar reasons as with the aqueous *d*-SiCNW electrode where doping was finely tuned for achieving dual enhanced electrical conductivity and the crucial quantum capacitance.

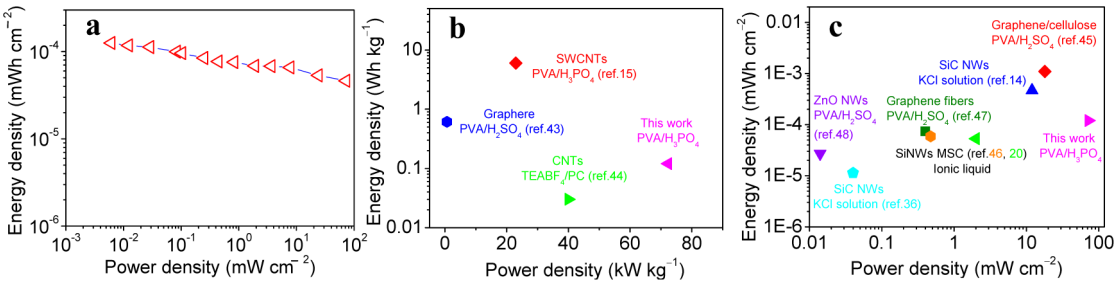

Figure 7. Energy and power densities of *d*-SiCNW−TSCs. (a) Ragone plot of *d*-SiCNW−TSCs measured in gelled electrolyte and (b and c) its corresponding data compared with other representative nanostructure-based SCs. *d*-SiCNW−TSCs exhibit exceptional electrochemical energy storage with simultaneous ultrahigh power density.

Their ordered porous structures in the sandwich-type architecture of the devices also have some parallels to the ideal nanoarray-based structures, which can both effectively absorb the gelled electrolyte and act as an electrolyte reservoir to facilitate ion transport and minimize its mean diffusion distance to the interior surfaces.[42] Another electrode-specific factor features a binder-free-TSC, which ramps up the electrochemical response rate with a reduction in the interfacial resistance.

One outstanding property that the *d*-SiCNW−TSC displays exceptionally well is its ability to be bent and twisted without affecting either its structural components or functional integrity in perfect unison, Figure 6a. To demonstrate the durability of *d*-SiCNWs for flexible energy storage, we tested their electrochemical performance under constant strain at a given scan rate, 1000 mV s^{-1}, Figure 6b. It is revealed most clearly the *d*-SiCNW−TSC exhibits exceptional electrochemical stability with only minute change in the device capacitance regardless of bending or twisting, indicating excellent mechanical stability; ditto the device tested while keeping the device under the bent or twisted state, Figure 6f. Remarkably, the capacitance was reversibly maintained, 98% retention of its initial capacitance as with its free-standing states after 2000 cycles, Figure S18. This superior performance makes *d*-SiCNW−TSCs promising for flexible-textile-electronics applications. The performance durability of the *d*-SiCNW−TSCs can be attributed to the highly mechanical flexibility of the electrodes combined with the interpenetrating porous network between two nanoarrays and the gelled electrolyte. The polymer-based electrolyte in TSCs becomes macromolecularly cross-linked after solidification and acts like a glue that closely holds all the TSC components together, thereby improving the mechanical integrity and increasing its calendar life even when tested under extreme bending/twisting conditions.

In fact, the total energy of a single supercapacitor is so low that supercapacitors must be connected in series and/or parallel configurations, just as batteries are, to form a "bank" with a specific voltage and capacitance rating. The adaptability of *d*-SiCNW−TSC for serial/parallel connections with four similar devices is demonstrated in Figure 6g−i. The tandem TSCs run very well regarding controlling over their operating voltage windows and capacitances, thus enabling them to be promising for futuristic applications, Figures S19−21. For example, the serial and parallel connections extend the output voltage and discharge time to 3.2 V and 5.2 s (*versus* 1 V and 1.2 s for a single device), respectively, whereas the output voltage and current can both be doubled with the serial−parallel connection. All the device assemblies exhibit essentially ideal charge/discharge triangular shapes with a minute voltage drop, again suggesting the ultrafast rate performance with minus internal resistance. Note that this exceptional characteristic is attained with no help from a voltage balance, which is often used with series combinations to prevent any cell from going into overvoltage.

To evaluate the overall performance of the *d*-SiCNW−TSCs for high-power fabric-electronics, a Ragone plot is shown in Figure 7. The results revealed that the *d*-SiCNW−TSC can exhibit energy densities of up to 1.2×10^{-4} mW·h cm^{-2} (0.13 W·h kg^{1-}), a value that is approximately two times higher than that of the AC-SC. Significantly, the device delivered an ultrahigh power density of 72.3 mW cm^{-2} (77.7 kW kg^{1-}) at a current density of 30 mA cm^{-2}, which is comparable to those of the reported results for 1D nanostructure CNTs or graphenes based SCs and the aluminum electrolytic capacitor, while providing more than 3 orders of magnitude higher energy density of the latter, further demonstrating the excellent rate performance of *d*-SiCNW−TSCs.

CONCLUSIONS

We have successfully demonstrated a single crystalline nitrogen-doped 3*C*-SiC nanoarray as a new-type single system of the most integrated merits for flexible energy-storage devices. The ability to be doped, charged, bent and superior-in-arbitrary-environment enabled as-prepared *d*-SiCNW−TSCs shows ultra high-power capability in both aqueous and gelled electrolytes along with excellent rate ability, cycle stability, durability to be bent, as well as being environmentally friendly. *d*-SiCNWs, thus, offer an entirely different type of

nanoarray-based electroactive material with enhanced functionality and reliability, and could find applications as integrated energy-storage units in textile and various portable electronics.

METHODS

3*C*-SiCNW Arrays Preparation. We took advantage of the catalysis-assisted pyrolysis method to synthesize our 3*C*-SiCNW array by using the commercially available polysilazane (Ceraset, Kion) as raw material.[29,49] The precursor was first solidified by heat-treatment at 260 °C for 30 min and then ground into powder and put into a graphite crucible. Then, 3 wt % $Co(NO_3)_3$ was introduced as the catalyst into the powder by adding the ethanol solution of $Co(NO_3)_3$ at a 0.2 mol L^{-1} concentration. The obtained powder mixture was pyrolyzed at 1550 °C for 30 min in a conventional furnace with a graphite resistance heater under well mixed ultrahigh purity N_2 (99.99%)/Ar (99.99%) at a flow rate of 200 sccm, followed by furnace-cooling to ambient temperature; the control and doped nanostructures obtained by independent control of N_2 content at 0, 1, 3, and 5% are named *c*-SiCNWs and *d*-SiCNWs, respectively. A carbon fabric with a thickness of ~80 μm was utilized as the substrate for sample preparation and placed on the top of the graphite crucible. Note that, during the high-temperature pyrolysis, we carefully calibrated the mixed gas pressure by keeping it at 0.15 MPa for 10 min and then reducing it to 0.11 MPa over 5 min, and keeping it constant for 15 min. Finally, the resulting products were immersed in respective dilute nitric acid and HF aqueous solutions to remove both the catalyst at the tips of wires and the exposed SiO_2 layer from the nanowires.

For the characterization on the bulk N dopant atomic concentration of SiCNWs, we combined two physical approaches that resolve the nitrogen content in SiCNWs: a X-ray fluorescence microscopy probe for silicon and an oxygen/nitrogen analyzer for nitrogen elemental analysis with high sensitivity on a large scale. The N content in five SiCNWs series was determined to be ~0, ~2, ~3, ~3, and ~5 atom %, respectively.

The characterization experiments on the electrochemical performances of the as-made electrodes in solution were carried out in a 3 M KCl aqueous electrolyte with a Pt wire counter electrode and Ag/AgCl reference electrode (filled with 1 M KCl with potential of 0.236 V *versus* standard hydrogen electrode). The all-solid-state flexible supercapacitors were produced by directly immersing two pieces of nanoarray electrodes into the poly(vinyl alcohol) ($PVA-H_3PO_4$) gelled electrolyte for 5 min and then assembled them together in the sandwich-structure with a separator (Whatman 8 μm filter paper) sandwiched in between and kept at ambient condition. The $PVA-H_3PO_4$ electrolyte was simply made as follows: 6 g H_3PO_4 was mixed with 60 mL deionized water and then 6 g PVA powder was added. Then, the whole mixture was heated to 85 °C under vigorous stirring until the solution became clear.

Conflict of Interest: The authors declare no competing financial interest.

Acknowledgment. This work was supported by the National Natural Science Foundation of China (Grant No. 51172112, 51272112 and 51472128).

Supporting Information Available: The Supporting Information is available free of charge on the ACS Publications website at DOI: 10.1021/acsnano.5b01784.

Characterization methods and calculations; additional structure and morphology characterization for the carbon fabric and SiCNWs; XPS survey, conductivity and porosity characterization as well as the electrochemical performance for SiCNW electrodes; elemental analysis for SiCNWs (PDF)

REFERENCES AND NOTES

1. Miller, J. R.; Simon, P. Electrochemical Capacitors for Energy Management. *Science* **2008**, *321*, 651–652.
2. Rogers, J. A.; Huang, Y. G. A Curvy, Stretchy Future for Electronics. *Proc. Natl. Acad. Sci. U. S. A.* **2009**, *106*, 10875–10876.
3. Simon, P.; Gogotsi, Y. Materials for Electrochemical Capacitors. *Nat. Mater.* **2008**, *7*, 845–854.
4. Arico, A. S.; Bruce, P.; Scrosati, B.; Tarascon, J. M.; Van Schalkwijk, W. Nanostructured Materials for Advanced Energy Conversion and Storage Devices. *Nat. Mater.* **2005**, *4*, 366–377.
5. Chmiola, J.; Yushin, G.; Gogotsi, Y.; Portet, C.; Simon, P.; Taberna, P. L. Anomalous Increase in Carbon Capacitance at Pore Sizes Less Than 1 Nanometer. *Science* **2006**, *313*, 1760–1763.
6. Lang, X. Y.; Hirata, A.; Fujita, T.; Chen, M. W. Nanoporous Metal/Oxide Hybrid Electrodes for Electrochemical Supercapacitors. *Nat. Nanotechnol.* **2011**, *6*, 232–236.
7. Merlet, C.; Rotenberg, B.; Madden, P. A.; Taberna, P.-L.; Simon, P.; Gogotsi, Y.; Salanne, M. On the Molecular Origin of Supercapacitance in Nanoporous Carbon Electrodes. *Nat. Mater.* **2012**, *11*, 306–310.
8. Peng, X.; Peng, L.; Wu, C.; Xie, Y. Two Dimensional Nanomaterials for Flexible Supercapacitors. *Chem. Soc. Rev.* **2014**, *43*, 3303–3323.
9. Li, H.; Zhao, Q.; Wang, W.; Dong, H.; Xu, D.; Zou, G.; Duan, H.; Yu, D. Novel Planar-Structure Electrochemical Devices for Highly Flexible Semitransparent Power Generation/Storage Sources. *Nano Lett.* **2013**, *13*, 1271–1277.
10. Chen, S.; Zhu, J.; Wu, X.; Han, Q.; Wang, X. Graphene Oxide–MnO_2 Nanocomposites for Supercapacitors. *ACS Nano* **2010**, *4*, 2822–2830.
11. Wang, H.; Zhang, L.; Tan, X.; Holt, C. M. B.; Zahiri, B.; Olsen, B. C.; Mitlin, D. Supercapacitive Properties of Hydrothermally Synthesized Co_3O_4 Nanostructures. *J. Phys. Chem. C* **2011**, *115*, 17599–17605.
12. Xu, H.; Hu, X.; Yang, H.; Sun, Y.; Hu, C.; Huang, Y. H. Flexible Asymmetric Micro-Supercapacitors Based on Bi_2O_3 and MnO_2 Nanoflowers: Larger Areal Mass Promises Higher Energy Density. *Adv. Energy Mater.* **2015**, *5*, 5.
13. Gu, L.; Wang, Y.; Lu, R.; Wang, W.; Peng, X.; Sha, J. Silicon Carbide Nanowires@$Ni(OH)_2$ Coreshell Structures on Carbon Fabric for Supercapacitor Electrodes with Excellent Rate Capability. *J. Power Sources* **2015**, *273*, 479–485.
14. Gu, L.; Wang, Y.; Fang, Y.; Lu, R.; Sha, J. Performance Characteristics of Supercapacitor Electrodes Made of Silicon Carbide Nanowires Grown on Carbon Fabric. *J. Power Sources* **2013**, *243*, 648–653.
15. Kaempgen, M.; Chan, C. K.; Ma, J.; Cui, Y.; Gruner, G. Printable Thin Film Supercapacitors Using Single-Walled Carbon Nanotubes. *Nano Lett.* **2009**, *9*, 1872–1876.
16. Niu, Z.; Dong, H.; Zhu, B.; Li, J.; Hng, H. H.; Zhou, W.; Chen, X.; Xie, S. S. Highly Stretchable, Integrated Supercapacitors Based on Single-Walled Carbon Nanotube Films with Continuous Reticulate Architecture. *Adv. Mater.* **2013**, *25*, 1058–1064.
17. El-Kady, M. F.; Strong, V.; Dubin, S.; Kaner, R. B. Laser Scribing of High-Performance and Flexible Graphene-Based Electrochemical Capacitors. *Science* **2012**, *335*, 1326–1330.
18. Wu, Z.-S.; Parvez, K.; Feng, X.; Müllen, K. Graphene-Based In-Plane Micro-Supercapacitors with High Power and Energy Densities. *Nat. Commun.* **2013**, *4*, 2487.
19. Yang, P.; Xiao, X.; Li, Y.; Ding, Y.; Qiang, P.; Tan, X.; Mai, W.; Lin, Z.; Wu, W.; Li, T.; Jin, H.; Liu, P.; Zhou, J.; Wong, C. P.; Wang, Z. L. Hydrogenated ZnO Core–Shell Nanocables for Flexible Supercapacitors and Self-Powered Systems. *ACS Nano* **2013**, *7*, 2617–2626.
20. Aradilla, D.; Gentile, P.; Bidan, G.; Ruiz, V.; Gómez-Romero, P.; Schubert, T. J. S.; Sahin, H.; Frackowiak, E.; Sadki, S. High

Performance of Symmetric Micro-Supercapacitors based on Silicon Nanowires Using N-methyl-N-propylpyrrolidinium bis (Trifluoromethylsulfonyl)imide as Electrolyte. *Nano Energy* **2014**, *9*, 273–281.
21. Chen, P.; Chen, H.; Qiu, J.; Zhou, C. Inkjet Printing of Single-Walled Carbon Nanotube/RuO_2 Nanowire Supercapacitors on Cloth Fabrics and Flexible Substrates. *Nano Res.* **2010**, *3*, 594–603.
22. Yuan, L.; Lu, X.-H.; Xiao, X.; Zhai, T.; Dai, J.; Zhang, F.; Hu, B.; Wang, X.; Gong, L.; Chen, J.; Hu, C.; Tong, Y.; Zhou, J.; Wang, Z. L. Flexible Solid-State Supercapacitors Based on Carbon Nanoparticles/MnO_2 Nanorods Hybrid Structure. *ACS Nano* **2012**, *6*, 656–661.
23. Lu, X.; Dou, H.; Yuan, C.; Yang, S.; Hao, L.; Zhang, F.; Shen, L.; Zhang, L.; Zhang, X. Polypyrrole/Carbon Nanotube Nanocomposite Enhanced the Electrochemical Capacitance of Flexible Graphene Film for Supercapacitors. *J. Power Sources* **2012**, *197*, 319–324.
24. Wang, K.; Zou, W.; Quan, B.; Yu, A.; Wu, H.; Jiang, P.; Wei, Z. An All-Solid-State Flexible Micro-Supercapacitor on a Chip. *Adv. Energy Mater.* **2011**, *1*, 1068–1072.
25. Chmiola, J.; Largeot, C.; Taberna, P.-L.; Simon, P.; Gogotsi, Y. Monolithic Carbide-Derived Carbon Films for Micro-Supercapacitors. *Science* **2010**, *328*, 480–483.
26. Miller, J. R.; Outlaw, R. A.; Holloway, B. C. Graphene Double-Layer Capacitor with ac Line-Filtering Performance. *Science* **2010**, *329*, 1637–1639.
27. Zhang, L. L.; Zhao, X.; Ji, H.; Stoller, M. D.; Lai, L.; Murali, S.; Mcdonnell, S.; Cleveger, B.; Wallace, R. M.; Ruoff, R. S. Nitrogen Doping of Graphene and Its Effect on Quantum Capacitance, and a New Insight on the Enhanced Capacitance of N-Doped Carbon. *Energy Environ. Sci.* **2012**, *5*, 9618–9625.
28. Lu, X.; Zhai, T.; Zhang, X.; Shen, Y.; Yuan, L.; Hu, B.; Gong, L.; Chen, J.; Gao, Y.; Zhou, J.; Tong, Y.; Wang, Z. L. WO_{3-x}@Au@MnO_2 Core–Shell Nanowires on Carbon Fabric for High-Performance Flexible Supercapacitors. *Adv. Mater.* **2012**, *24*, 938–944.
29. Zhang, X. N.; Chen, Y. Q.; Liu, W.; Xue, W. J.; Li, J. H.; Xie, Z. P. Growth of n-type 3C-SiC Nanoneedles on Carbon Fabric: Toward Extremely Flexible Field Emission Devices. *J. Mater. Chem. C* **2013**, *1*, 6479–6486.
30. Wong, E. W.; Sheehan, P. E.; Lieber, C. M. Nanobeam Mechanics: Elasticity, Strength, and Toughness of Nanorods and Nanotubes. *Science* **1997**, *277*, 1971–1975.
31. Casady, J. B.; Johnson, R. W. Status of Silicon Carbide (SiC) as a Wide-Bandgap Semiconductor for High-Temperature Applications. *Solid-State Electron.* **1996**, *39*, 1409–1422.
32. Fan, J. Y.; Wu, X. L.; Chu, P. K. Low-Dimensional SiC Nanostructures: Fabrication, Luminescence, and Electrical Properties. *Prog. Mater. Sci.* **2006**, *51*, 983–1031.
33. Zhang, X. N.; Chen, Y. Q.; Xie, Z. P.; Yang, W. Y. Shape and Doping Enhanced Field Emission Properties of Quasialigned 3C-SiC Nanowires. *J. Phys. Chem. C* **2010**, *114*, 8251–8255.
34. Chen, Y. Q.; Zhang, X. N.; Zhao, Q.; He, L.; Huang, C. K.; Xie, Z. P. P-type 3C-SiC Nanowires and Their Optical and Electrical Transport Properties. *Chem. Commun.* **2011**, *47*, 6398–6400.
35. Song, B.; Bao, H. Q.; Li, H.; Lei, M.; Peng, T. H.; Jian, J. K.; Liu, J.; Wang, W. Y.; Wang, W. J.; Chen, X. L. Observation of Glassy Ferromagnetism in Al-doped 4H-SiC. *J. Am. Chem. Soc.* **2009**, *131*, 1376–1377.
36. Alper, J. P.; Kim, M. S.; Vincent, M.; Hsia, B.; Radmilovic, V.; Carraro, C.; Maboudian, R. Silicon Carbide Nanowires as Highly Robust Electrodes for Microsupercapacitors. *J. Power Sources* **2013**, *230*, 298–302.
37. Kohlscheen, J.; Emirov, Y. N.; Beerbom, M. M.; Wolan, J. T.; Saddow, S. E.; Chung, G.; MacMillan, M. F.; Schlaf, R. Band Line-Up Determination at p- and n-type Al/4H-SiC Schottky Interfaces Using Photoemission Spectroscopy. *J. Appl. Phys.* **2003**, *94*, 3931–3938.
38. Pech, D.; Brunet, M.; Durou, H.; Huang, P.; Mochalin, V.; Gogotsi, Y.; Taberna, P.-L.; Simon, P. Ultrahigh-Power Micrometre-Sized Supercapacitors Based on Onion-Like Carbon. *Nat. Nanotechnol.* **2010**, *5*, 652–654.
39. Thissandier, F.; Dupré, L.; Gentile, P.; Brousse, T.; Bidan, G.; Buttard, D.; Sadki, S. Ultra-Dense and Highly Doped SiNWs for Micro-Supercapacitorselectrodes. *Electrochim. Acta* **2014**, *117*, 159–163.
40. Lu, X.; Yu, M.; Wang, G.; Zhai, T.; Xie, S.; Ling, Y.; Tong, Y.; Li, Y. H-TiO_2 @MnO_2 //H-TiO_2 @C Core–Shell Nanowires for High Performance and Flexible Asymmetric Supercapacitors. *Adv. Mater.* **2013**, *25*, 267–272.
41. Beidaghi, M.; Wang, C. Micro-Supercapacitors Based on Interdigital Electrodes of Reduced Graphene Oxide and Carbon Nanotube Composites with Ultra High Power Handling Performance. *Adv. Funct. Mater.* **2012**, *22*, 4501–4510.
42. Wang, D.-W.; Li, F.; Liu, M.; Lu, G. Q.; Cheng, H.-M. 3D Aperiodic Hierarchical Porous Graphitic Carbon Material for High-Rate Electrochemical Capacitive Energy Storage. *Angew. Chem., Int. Ed.* **2008**, *47*, 373–376.
43. Xu, Y.; Lin, Z.; Huang, X.; Liu, Y.; Huang, Y.; Duan, X. Flexible Solid-State Supercapacitors Based on Three-Dimensional Graphene Hydrogel Films. *ACS Nano* **2013**, *7*, 4042–4049.
44. Masarapu, C.; Zeng, H. F.; Hung, K. H.; Wei, B. Q. Effect of Temperature on the Capacitance of Carbon Nanotube Supercapacitors. *ACS Nano* **2009**, *3*, 2199–2206.
45. Weng, Z.; Su, Y.; Wang, D. W.; Li, F.; Du, J.; Cheng, H. M. Graphene–Cellulose Paper Flexible Supercapacitors. *Adv. Energy Mater.* **2011**, *1*, 917–922.
46. Berton, N.; Brachet, M.; Thissandier, F.; Bideau, J. L.; Gentile, P.; Bidan, G.; Brousse, T.; Sadki, S. Wide-Voltage-Window Silicon Nanowire Electrodes for Micro-Supercapacitors *via* Electrochemical Surface Oxidation in Ionic Liquid Electrolyte. *Electrochem. Commun.* **2014**, *41*, 31–34.
47. Bae, J.; Song, M. K.; Park, Y. J.; Kim, J. M.; Liu, M.; Wang, Z. L. Fiber Supercapacitors Made of Nanowire-Fiber Hybrid Structures for Wearable/Flexible Energy Storage. *Angew. Chem., Int. Ed.* **2011**, *50*, 1683–1687.
48. Li, X. M.; Zhao, T.; Chen, Q.; Li, P.; Wang, K.; Zhong, M.; Wei, J.; Wu, D.; Wei, B.; Zhu, H. W. Flexible All Solid-state Supercapacitors Based on Chemical Vapor Deposition Derived Graphene Fibers. *Phys. Chem. Chem. Phys.* **2013**, *15*, 17752–17757.
49. Dhamne, A.; Xu, W. X.; Fookes, B. G.; Fan, Y.; Zhang, L. G.; Burton, S.; Hu, J. Z.; Ford, J.; An, L. N. Polymer–Ceramic Conversion of Liquid Polyaluminasilazanes for SiAlCN Ceramics. *J. Am. Ceram. Soc.* **2005**, *88*, 2415–2419.